Consideration of radial dependences of axial stresses in the shear-lag model for fibre pull-out

C.-H. HSUEH
Metals and Ceramics Division, Oak Ridge National Laboratory, Oak Ridge, TN 37831, USA

The shear-lag model has been used extensively to analyse stress transfer during single-fibre pull-out. To achieve analytical solutions, the radial dependences of the axial stresses in the fibre and the matrix are generally ignored in the shear-lag model. The present study considered these radial dependence in the shear-lag model. The differences between the predictions obtained by ignoring these radial dependences, considering the radial dependence of the axial stress in the fibre only, considering the radial dependence of the axial stress in the matrix only, and considering both radial dependences, have been addressed.

1. Introduction
Optimum toughening of a fibre-reinforced ceramic composite requires debonding at fibre–matrix interfaces before fibre fracture as the main crack extends through the composite [1, 2]. Fibre pull-out tests [3–5] are often used to evaluate the interfacial properties of composites. The condition of interfacial debonding has been defined by two criteria: the shear strength criterion [5–7] and the critical energy release rate criterion [8–10]. In the former, the shear-lag model has been used extensively to derive the maximum interfacial shear stress, which is then compared to the interfacial shear strength. Interfacial debonding occurs when the maximum interfacial shear stress reaches the interfacial shear strength before the applied axial stress on the fibre reaches the fibre strength.

An analytical solution of the stress transfer during fibre pull-out is difficult to obtain, especially when the interface is bonded and the stress transfer is high (i.e. the stress gradient is high) near the loaded region. To derive analytical solutions in the shear-lag model [5–8, 11–16], approximations are required. Various theoretical analyses for this stress transfer problem have been reviewed [17]. Generally, the radial dependences of the axial stresses in both the fibre and the matrix are ignored in the analyses (i.e. the classical shear-lag model) [5, 6, 8, 10–14]. With this simplification, the difficulty in obtaining an analytical solution is greatly reduced. However, two exceptions to this simplification exist. (1) When the radial dimension of the matrix is similar to that of the fibre (i.e. the matrix becomes a thin coating), the radial dependence of the axial stress in the fibre has been considered [16]. (2) When the radial dimension of the matrix is much greater than that of the fibre (which is generally valid for fibre pull-out tests), the radial dependence of the axial stress in the matrix has been considered [7, 15].

Recently, a modified shear-lag model was developed in which the radial dependence of axial stresses in both the fibre and the matrix were included in the analysis [18]. However, the approximations adopted in the equilibrium equation in stress analyses were not clarified, and the results obtained from the classical shear-lag model, which is more widely accepted, were not included for comparison. As a complement to that work [18], the purpose of the present study was to address the approximations adopted in the modified shear-lag model, and to include the results obtained from the classical shear-lag model for comparison. The problem of assuming a constant interfacial shear stress along a bonded interface in analysing the experimental results has also been considered.

2. The shear-lag model
The idealized specimen for the single-fibre pull-out test (i.e. the shear-lag model) is shown in Fig. 1. A fibre with a radius a, is located at the centre of a coaxial cylindrical shell of matrix with an outer radius b, and a thickness t. The radial and the axial coordinates are r and z, respectively. The fibre is subjected to an applied axial stress, σ_0, at one end of the specimen (i.e. at $z = t$ in Fig. 1). The stress transfers from the fibre to the matrix through the interfacial shear stress, τ_i, such that the fibre is free of stress at $z = 0$. The results derived from previous shear-lag models (see Fig. 2a–c) are summarized and discussed in this section. For the modified shear-lag model (Fig. 2d), the approximations adopted and the results derived are presented in Section 3.

It is noted that analytical analyses in the shear-lag model are unable to handle the complicated singularity, which occurs at $z = t$ for a bonded interface [19–21]. To avoid this singularity, a finite element analysis has been performed by assuming that the applied load is distributed over the inner 50% of the fibre diameter [22]. By using an average axial stress technique, this singularity is also avoided [23]. Both results [22, 23] show that τ_i is zero at the loaded surface, increases and reaches a maximum value at a relatively short distance (about 0.4 times [22] and 0.25 times [23] the fibre diameter, respectively) below
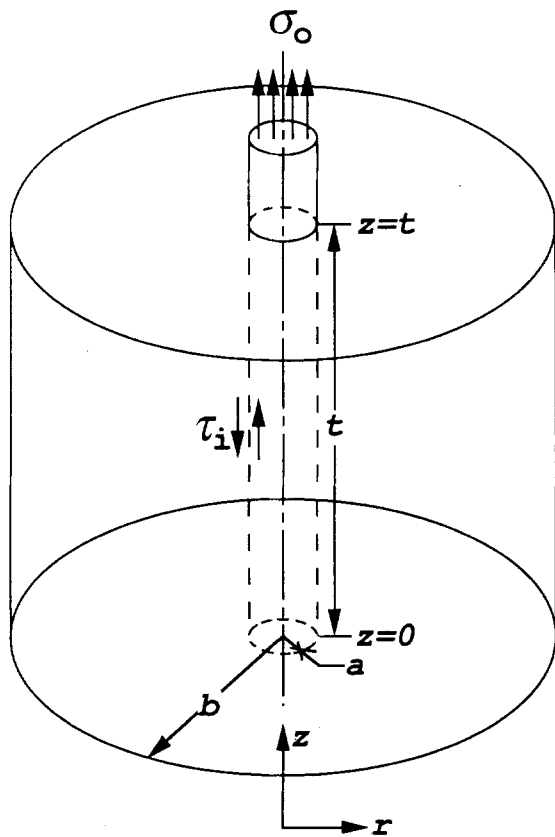
Figure 1 Schematic drawing of the shear-lag model used in analysing the stress transfer from the fibre to the matrix during fibre pull-out.
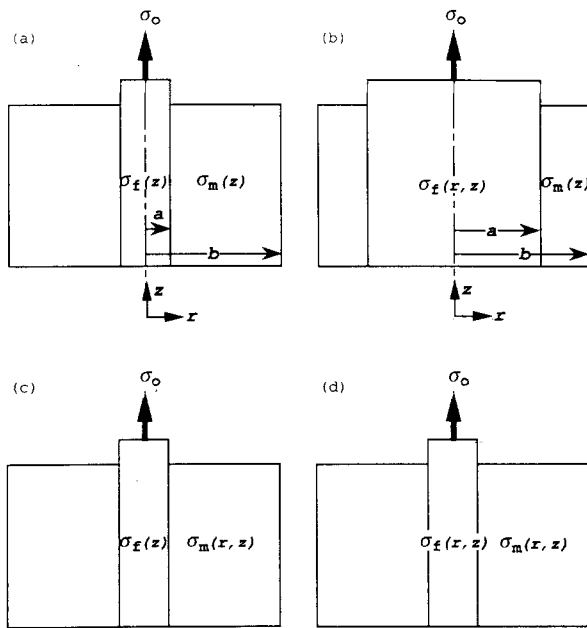

Figure 2 Schematic drawings showing (a) the classical shear-lag model, (b) the fibre/coating system where $(b - a) \ll a$, (c) the fibre/matrix system where $b \gg a$, and (d) the modified shear-lag model.

the loaded surface. In addition, the maximum interfacial shear stress obtained from the finite element analysis is approximately equal to that obtained from the shear-lag model [22]. The maximum interfacial shear stress occurs at $z = t$, based on the shear-lag model, and has been used extensively to define the shear strength debonding criterion.

2.1. Predictions obtained by ignoring radial dependences of axial stresses: the classical shear-lag model

The radial dependences of axial stresses in both the fibre and the matrix are ignored in the classical shear-lag model (Fig. 2a). The maximum interfacial shear stress, τ_0, which occurs at $z = t$, is [5, 6]

$$\tau_0 = -\frac{\sigma_0}{2}\left[\frac{E_m}{(1 + v_m)E_f \ln(b/a)}\right]^{1/2} \coth(\beta t) \quad (1)$$

where E and v are Young's modulus and Poisson's ratio, and the subscripts f and m denote the fibre and the matrix, respectively. The coefficient β is given by

$$\beta = \frac{1}{a}\left[\frac{E_m}{(1 + v_m)E_f \ln(b/a)}\right]^{1/2} \quad (2)$$

2.2. Predictions obtained by considering the radial dependence of the axial stress in the fibre only: fibre/coating

When the radial dimension of the matrix is similar to that of the fibre (i.e. the matrix becomes a thin coating), the radial dependence of the axial stress in the fibre has been considered [16]. The radial dependence of the axial stress in the coating is ignored due to the relatively small radial dimension of the coating compared to that of the fibre. However, a difference exists between Fig. 2b and the geometry considered elsewhere [16]. The system considered previously [16] is that a fibre has a uniform coating along its central portion and an axial tensile stress is applied at both bare ends of the fibre. The solution pertinent to the system depicted in Fig. 2b can be obtained by adopting the analysis in [16] and replacing the free surface condition for both ends of the coating by the following two boundary conditions

$$\sigma_m = 0 \qquad \text{at } z = t \qquad (3a)$$

$$\sigma_m = \frac{a^2 \sigma_0}{b^2 - a^2} \qquad \text{at } z = 0 \qquad (3b)$$

where σ_m is the axial stress in the matrix (i.e. the coating). The solution of the maximum interfacial shear stress in Fig. 2b for the case of $(b - a) \ll \iota$ becomes

$$\tau_0 = -\sigma_0 \left\{\frac{(b^2 - a^2)E_m}{(1 + v_f)[a^2 E_f + (b^2 - a^2)E_m]}\right\}^{1/2}$$

$$\times \left\{\coth(\alpha_1 t)\right.$$

$$+ \frac{2a^2 E_f}{(b^2 - a^2)E_m[\exp(\alpha_1 t) - \exp(-\alpha_1 t)]}\right\} \quad (4)$$

where α_1 is given by

$$\alpha_1 = \frac{2}{a}\left[\frac{a^2 E_f + (b^2 - a^2)E_m}{(b^2 - a^2)(1 + v_f)E_m}\right]^{1/2} \quad (5)$$

2.3. Predictions obtained by considering the radial dependence of the axial stress in the matrix only: fibre/matrix

The radial dimension of the matrix is generally much greater than that of the fibre in the fibre pull-out tests. Hence, the radial dependence of the axial stress is considered in the matrix but is ignored in the fibre (Fig. 2c) [7, 15]. The solution of the maximum interfacial shear stress obtained is [7, 15]

$$\tau_0 = \frac{-\sigma_0(b^2 - a^2)E_m\{\coth(\alpha_2 t) + 2a^2 E_f/(b^2 - a^2)E_m[\exp(\alpha_2 t) - \exp(-\alpha_2 t)]\}}{2\left\{(1 + v_m)E_f[a^2 E_f + (b^2 - a^2)E_m]\left[b^2 \ln\left(\frac{b}{a}\right) - \frac{b^2 - a^2}{2}\right]\right\}^{1/2}} \tag{6}$$

where α_2 is given by

$$\alpha_2 = \frac{1}{a}\left\{\frac{a^2 E_f + (b^2 - a^2)E_m}{(1 + v_m)E_f[b^2 \ln(b/a) - (b^2 - a^2)/2]}\right\}^{1/2} \tag{7}$$

It is noted that the approximated shear stress in the matrix adopted in the analysis [7, 15] does not satisfy the free surface condition at $r = b$. However, the error due to this approximate shear stress decreases when b/a increases [24], and $b \gg a$ is the condition for the fibre matrix system. It has been shown earlier [15] that when $b/a = 10$, the analytical solution obtained [15] is in excellent agreement with the numerical solution obtained by Muki and Sternberg [25] for the axial stress distribution in the fibre.

3. The modified shear-lag model

Compared to the analysis for the fibre/matrix system, the analysis for the modified shear-lag model contains three modifications: (1) the radial dependence of the axial stress in the fibre is included (i.e. not ignored); (2) the shear stress distribution in the matrix satisfies exactly (i.e. not approximately) the free surface condition at $r = b$, and (3) the exact equilibrium equation (as compared to the plane strain condition) is used to relate the tangential stress to the radial stress at the interface. To obtain analytical solutions, the approximations adopted earlier [18] are discussed below.

For an axial symmetric geometry, which has the cylindrical polar coordinates, r, θ and z, the equilibrium equations between the normal and the shear stresses (i.e. σ and τ) are [26]

$$\frac{\partial \sigma_z}{\partial z} + \frac{1}{r}\frac{\partial(r\tau_{rz})}{\partial r} = 0 \tag{8a}$$

$$\frac{\partial \sigma_r}{\partial r} + \frac{\partial \tau_{rz}}{\partial z} + \frac{\sigma_r - \sigma_\theta}{r} = 0 \tag{8b}$$

To satisfy strictly the equilibrium equations, the stress–displacement relation, and the essential boundary conditions, solutions for the stress-transfer problem require extensive numerical analysis. Owing to the nature of the approximate analytical solution, it is impossible to satisfy exactly all the required conditions for the fibre pull-out problem [23]. Substitution of the shear stress from Equations 9 or 10 in [18] into Equation 8a results in a radial-independent axial

stress, which should be regarded as an average value with respect to the radial coordinate [23]. In the modified shear-lag model [18], Equation 8a is satisfied in an average sense, such that

$$\frac{\partial \bar{\sigma}_z}{\partial z} + \frac{1}{r}\frac{\partial(r\tau_{rz})}{\partial r} = 0 \tag{8c}$$

is satisfied for both the fibre and the matrix. However, to relate the tangential stress to the radial stress at the interface, the equilibrium equation of Equation 8b is satisfied exactly (see Section 7.1 in [18]).

The solution of the average axial stress in the fibre, $\bar{\sigma}_f$, obtained is [18]

$$\begin{aligned}
\bar{\sigma}_f = &\left\{\sigma_0 \Big/ \left[1 + \frac{b^2 - a^2}{a^2}\left(\frac{P_1 E_m}{E_f} - P_3\right)\right]\right\} \\
&\times \left\{\left[1 - \frac{(b^2 - a^2)P_3}{a^2}\right] \right. \\
&\times \left[1 + \frac{\exp[-\alpha_3(t - z)] - \exp[\alpha_3(t - z)]}{\exp(\alpha_3 t) - \exp(-\alpha_3 t)}\right] \\
&\left. + \frac{(b^2 - a^2)P_1 E_m}{a^2 E_f}\frac{\exp(\alpha_3 z) - \exp(-\alpha_3 z)}{\exp(\alpha_3 t) - \exp(-\alpha_3 t)}\right\}
\end{aligned} \tag{9}$$

where P_1, P_2 and P_3 are defined by Equation 32a–c in [18], and

$$\begin{aligned}
\alpha_3 = &\frac{1}{a}\left\{[a^2 E_f + (b^2 - a^2)(P_1 E_m - P_3 E_f)]\Big/\right. \\
&\times \frac{b^2(1 + v_m)E_f}{b^2 - a^2}\left[b^2 \ln\left(\frac{b}{a}\right)\right. \\
&\left. - \frac{(b^2 - a^2)(3b^2 - a^2)}{4b^2}\right] + (b^2 - a^2) \\
&\left. \times \left[\frac{(1 + v_f)P_1 E_m}{4} + \frac{P_2 E_f}{2}\right]\right\}^{1/2}
\end{aligned} \tag{10}$$

The corresponding maximum interfacial shear stress, τ_0, is

$$\begin{aligned}
\tau_0 = &-\sigma_0(b^2 - a^2)P_1 E_m \\
&\times \left\{\coth(\alpha_3 t) + \left[1 - \frac{(b^2 - a^2)P_3}{a^2}\right]\right. \\
&\left. \times \left[\frac{2a^2 E_f}{(b^2 - a^2)P_1 E_m[\exp(\alpha_3 t) - \exp(-\alpha_3 t)]}\right]\right\}\Big/ \\
&\times 2\left\{[a^2 E_f + (b^2 - a^2)(P_1 E_m - P_3 E_f)]\right. \\
&\times \left[\frac{b^2(1 + v_m)E_f}{b^2 - a^2}\left(b^2 \ln\left(\frac{b}{a}\right) - \frac{(b^2 - a^2)(3b^2 - a^2)}{4b^2}\right)\right. \\
&\left.\left. + (b^2 - a^2)\left(\frac{(1 + v_f)P_1 E_m}{4} + \frac{P_2 E_f}{2}\right)\right]\right\}^{1/2}
\end{aligned} \tag{11}$$

The maximum interfacial shear stress derived based on various models (i.e. Equations 1, 4, 6 and 11 are compared in the following section.

4. Theoretical predictions

In the present study, $v_f = 0.2$ and $v_m = 0.25$ are used in the closed form analytical solutions to elucidate the essential trends. First, the calculated average axial stress in the fibre and shear stress distribution along the fibre length are shown. Then, the dependence of the applied stress required for initial debonding on the thickness of the pull-out specimen is examined. Finally, the maximum interfacial shear stresses predicted from the classical shear-lag model, the fibre/coating system, the fibre/matrix system, and the modified shear-lag model, are compared.

4.1. The stress distributions along the fibre length

The normalized average axial stress in the fibre, $\bar{\sigma}_f/\sigma_0$, and interfacial shear stress, τ_i/σ_0, as functions of the normalized axial position, $(t - z)/t$, are shown in Fig. 3a and b, respectively, for $E_f/E_m = 1$, and $b/a = 100$ at different values of t/a. When t/a decreases, the distribution of $\bar{\sigma}_f$ becomes more linear (Fig. 3a), and the interfacial shear stress becomes more uniform (Fig. 3b) along the fibre length. However, even when the thickness of the specimen equals the

fibre radius, variations of τ_i along the fibre length still exist.

Based on the interfacial shear strength debonding criterion, the interfacial shear strength should be obtained from the applied axial stress required to initiate debonding (i.e. the initial debond stress) and the relation between σ_0 and τ_0 (i.e. Equation 1, 4, 6 and 11). However, a simple assumption of a constant interfacial shear stress has been adopted elsewhere, such that the interfacial shear strength can be obtained readily from the initial debond stress, the radius of the fibre, and the thickness of the specimen. The results in Fig. 3b show that the assumption of a constant interfacial shear stress along the fibre length is generally not recommended.

4.2. The length dependence of the (initial) debond stress

The interfacial shear stress obtained has a negative sign for the coordinate system chosen in Fig. 1. However, the sign of the shear stress signifies the direction of shear. A positive interfacial shear strength, τ_s, is considered in the present study. Interfacial debonding occurs when τ_0 reaches τ_s, and the corresponding applied axial stress required is defined as σ_d. The calculated normalized debond stress, σ_d/τ_s, as a function of the normalized fibre length, t/a, is shown in Fig. 4 for $b/a = 100$ at different E_f/E_m ratios. The σ_d/τ_s ratio increases from zero and reaches a plateau when t/a increases. When E_f/E_m increases, both the plateau of σ_d/τ_s and the critical t/a ratio required to reach the plateau increase. For ceramic fibre-reinforced ceramic composites, the fibre and the matrix generally have similar Young's moduli. In this case, σ_d/τ_s reaches its plateau value at a fibre length of about five times the fibre radius (see Fig. 4), and experimental observation of the length dependence of the debond stress is generally difficult. However, the predicted trend of the length dependence of σ_d has been reported for SiC fibre-reinforced titanium [27]. A recent study of fibre pull-out of SiC fibre reinforced borosilicate glass [28] also supports this length dependence.
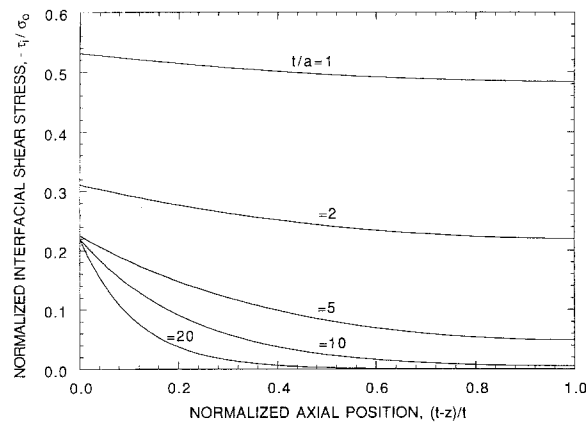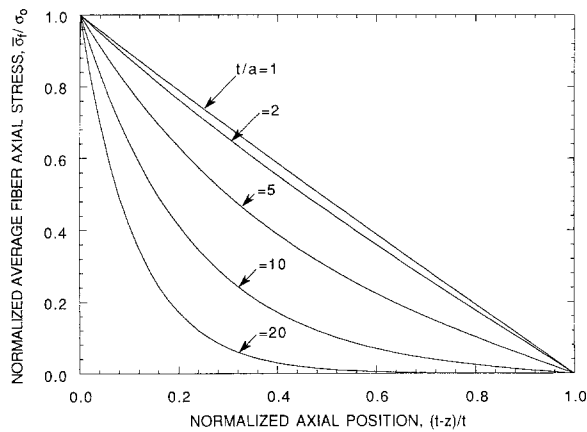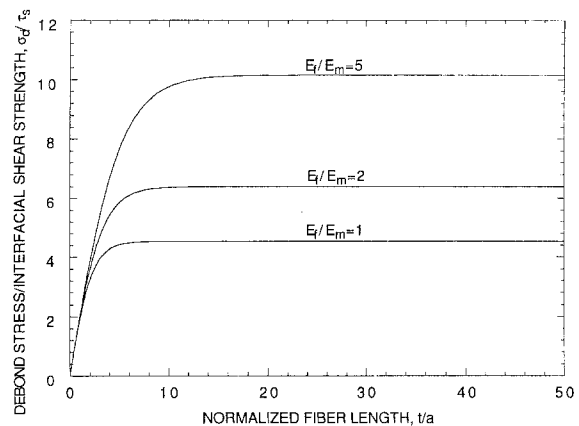
Figure 3 The normalized (a) average axial stress in the fibre, $\bar{\sigma}_f/\sigma_0$, and (b) interfacial shear stress, $-\tau_i/\sigma_0$, as functions of the normalized axial position, $(t - z)/t$, for $E_f/E_m = 1$, $v_f = 0.2$, $v_m = 0.25$, and $b/a = 100$ at different values of t/a.

Figure 4 The ratio of debond stress to interfacial shear strength, σ_d/τ_s, as a function of the normalized specimen thickness, t/a, for $v_f = 0.2$, $v_m = 0.25$, and $b/a = 100$ at different values of E_f/E_m.

4.3. Comparison

The maximum interfacial shear stress reaches its asymptote at relatively short fibre lengths (Fig. 4). Hence, the asymptote of τ_0 is considered for the purpose of comparison among different shear-lag models.

When the fibre length is sufficiently long, the asymptotes of τ_0 are

$$\tau_0 = -\frac{\sigma_0}{2}\left[\frac{E_m}{(1 + v_m)E_f \ln(b/a)}\right]^{1/2} \quad (12)$$

for the classical shear-lag model,

$$\tau_0 = -\sigma_0\left\{\frac{(b^2 - a^2)E_m}{(1 + v_f)[a^2 E_f + (b^2 - a^2)E_m]}\right\}^{1/2} \quad (13)$$

for the fibre/coating system,

$$\tau_0 = [-\sigma_0(b^2 - a^2)E_m]\Big/$$

$$\times 2\left\{(1 + v_m)E_f[a^2 E_f + (b^2 - a^2)E_m]\right.$$

$$\times \left.\left[b^2\ln\left(\frac{b}{a}\right) - \frac{b^2 - a^2}{2}\right]\right\}^{1/2} \quad (14)$$

for the fibre/matrix system, and

$$\tau_0 = [-\sigma_0(b^2 - a^2)P_1 E_m]\Big/$$

$$\times 2\left\{[a^2 E_f + (b^2 - a^2)(P_1 E_m - P_3 E_f)]\right.$$

$$\times \left[\frac{b^2(1 + v_m)E_f}{b^2 - a^2}\left(b^2\ln\left(\frac{b}{a}\right)\right.\right.$$

$$\left.\left.- \frac{(b^2 - a^2)(3b^2 - a^2)}{4b^2}\right) + (b^2 - a^2)\right.$$

$$\times \left.\left.\left(\frac{(1 + v_f)P_1 E_m}{4} + \frac{P_2 E_f}{2}\right)\right]\right\}^{1/2} \quad (15)$$

for the modified shear-lag model.

The calculated normalized asymptote of the maximum interface shear stress, $-\tau_0/\sigma_0$, as a function of
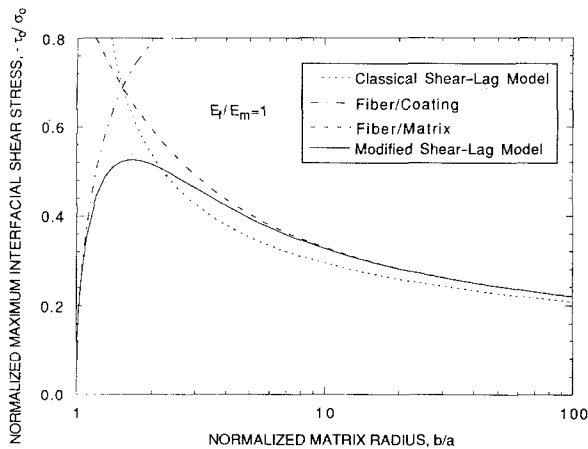

Figure 5 Comparison of the normalized maximum interfacial shear stress, $-\tau_0/\sigma_0$, with b/a for (- - -) the classical shear-lag model, (– - –) the fibre/coating system, (- - -) the fibre/matrix system, and (——) the modified shear-lag model, for $v_f = 0.2$, $v_m = 0.25$, $t/a = 50$, and $E_f/E_m = 1$.

b/a is shown in Fig. 5 for $E_f/E_m = 1$, and the following results are concluded. (1) The analysis in the fibre/coating system is appropriate when $(b - a) \ll a$, and its results approach those obtained from the modified shear-lag model when b/a is close to 1. (2) The analysis in the fibre/matrix system is applicable when $b \gg a$, and its results approach those obtained from the modified shear-lag model when b/a has large values. (3) The results obtained from the classical shear-lag model are similar to those from the fibre/matrix system when $b/a > 2$. However, compared to the classical shear-lag model, the results obtained from the fibre/matrix analysis show better agreement with the modified shear-lag model. (4) The modified shear-lag model considers the radial dependence of axial stresses in both the fibre and the matrix, and is applicable to the whole range of b/a. Also, when E_f/E_m increases (see Fig. 3 in [18]), the applicable range of b/a decreases for the fibre/coating analysis but increases for the fibre/matrix analysis.

5. Conclusion

To derive the analytical solution for the stress transfer during fibre pull-out, the radial dependences of the axial stresses in both the fibre and the matrix are generally ignored. Two efforts have been made to include the radial dependence of the axial stress in the analysis. (1) In the fibre/coating system [16], the radial dependence of the axial stress in the fibre is considered. (2) In the typical fibre pull-out test, the radial dimension of the matrix is much greater than the fibre, and the radial dependence of the axial stress in the matrix is considered [7]. The recently developed modified shear-lag model [18] considers the radial dependences of axial stresses in both the fibre and the matrix, and is applicable for any radial dimension of the matrix. Generally, the analysis in the fibre/matrix system [7] is applicable to the fibre pull-out test. However, in analysing the fibre-reinforced composite, a representative volume element is always chosen which has the same geometry of the single-fibre pull-out (Fig. 1), and the relative radial dimension of the fibre to the matrix (i.e. a/b in Fig. 1) is dictated by the square root of the volume fraction of fibres in the composite. In this case, the modified shear-lag model should be used when the volume fraction of fibres, a^2/b^2, is high in a composite. Finally, the residual stress is not included in the present analysis. In the presence of the residual radial and axial stresses, the analysis can be modified based on previously published reports [29, 30].

Acknowledgements

References

1. A. G. EVANS and R. M. McMEEKING, *Acta Metall.* **34** (1986) 2435.
2. P. F. BECHER, C. H. HSUEH, P. ANGELINI and T. N. TIEGS, *J. Am. Ceram. Soc.* **71** (1988) 1050.
3. E. P. BUTLER, E. R. FULLER Jr and H. M. CHAN, in "MRS Symposium Proceedings: Tailored Interfaces in Composite Materials", edited by C. G. Pantano and E. J. Chen, (Materials Research Society, Pittsburgh, PA, 1990) pp. 17–24.
4. J. D. BRIGHT, S. DANCHAIVIJIT and D. K. SHETTY, *J. Am. Ceram. Soc.* **74** (1991) 115.
5. A. TAKAKU and R. G. C. ARRIDGE, *J. Phys. D Appl. Phys.* **6** (1973) 2038.
6. P. LAWRENCE, *J. Mater. Sci.* **7** (1972) 1.
7. C. H. HSUEH, *Mater. Sci Eng.* **A123** (1990) 1.
8. Y. C. GAO, Y. W. MAI and B. COTTERELL, *J. Appl. Math. Phys. (ZAMP)* **39** (1988) 550.
9. J. P. OUTWATER and M. C. MURPHY, in "Proceedings of the 24th Annual Technical Conference of Reinforced Plastic/Composites Division". (The Society of the Plastics Industry Inc., Composites Division, New York, 1969). Paper 11c.
10. J. W. HUTCHINSON and H. M. JENSON, *Mech. Mater.* **9** (1990) 139.
11. H. L. COX, *Br. J. Appl. Phys.* **3** (1952) 72.
12. M. R. PIGGOTT, "Load Bearing Fibre Composites" (Pergamon Press, Elmsford, NY, 1980) p. 62.
13. B. BUDIANSKY, J. W. HUTCHINSON and A. G. EVANS, *J. Mech. Phys. Solids* **34** (1986) 167.
14. D. K. SHETTY, *J. Am. Ceram. Soc.* **71** (1988) C107.
15. C. H. HSUEH, *J. Mater. Sci. Lett.* **7** (1988) 497.
16. *Idem, J. Am. Ceram. Soc.* **71** (1988) 490.
17. R. J. KERANS and T. A. PARTHASARATHY, *ibid.* **74** (1991) 1585.
18. C. H. HSUEH, *Mater. Sci. Eng.* **A154** (1992) 125.
19. C. ATKINSON, J. AVILA, E. BETZ and R. E. SEMLSER, *J. Mech. Phys. Solids* **30** (1982) 97.
20. A. R. ZAK and M. L. WILLIAMS, *J. Appl. Mech.* **30** (1963) 142.
21. A. R. ZAK, *ibid.* **31** (1964) 150.
22. D. H. GRANDE, J. F. MANDELL and K. C. C. HONG, *J. Mater. Sci.* **23** (1988) 311.
23. L. N. McCARTNEY, *Proc. R. Soc. Lond.* **A425** (1989) 215.
24. C. H. HSUEH, *J. Mater. Sci. Lett.* **11** (1992) 1663.
25. R. MUKI and E. STERNBERG, *Int. J. Solids Struct.* **6** (1970) 69.
26. S. P. TIMOSHENKO and J. N. GOODIER, "Theory of Elasticity" (McGraw-Hill, New York, 1951) p. 380.
27. M. C. WATSON and T. W. CLYNE, *Acta Metall. Mater.* **40** (1992) 141.
28. J. K. KIM, C. BAILLIE and Y. W. MAI, *J. Mater. Sci.* **27** (1992) 3143.
29. C. H. HSUEH, *Mater. Sci. Eng.* **A145** (1991) 135.
30. *Idem, ibid.* **A145** (1991) 143.